ACS APPLIED MATERIALS & INTERFACES
RESEARCH ARTICLE
www.acsami.org

Bioinspired Aquatic Microrobot Capable of Walking on Water Surface Like a Water Strider

Xinbin Zhang,[†] Jie Zhao,[†] Qing Zhu,[‡] Ning Chen,[‡] Mingwen Zhang,[†] and Qinmin Pan*,[†,‡]

[†]State Key Laboratory of Robotics and System and [‡]School of Chemical Engineering and Technology, Harbin Institute of Technology, Harbin 150001, P.R. China

Supporting Information

ABSTRACT: Walking on the water surface is a dream of humans, but it is exactly the way of life for some aquatic insects. In this study, a bionic aquatic microrobot capable of walking on the water surface like a water strider was reported. The novel water strider-like robot consisted of ten superhydrophobic supporting legs, two miniature dc motors, and two actuating legs. The microrobot could not only stand effortlessly but also walk and turn freely on the water surface, exhibiting an interesting motion characteristic. A numerical model describing the interface between the partially submerged leg and the air—water surface was established to fully understand the mechanism for the large supporting force of the leg. It was revealed that the radius and water contact angle of the legs significantly affect the supporting force. Because of its high speed, agility, low cost, and easy fabrication, this microrobot might have a potential application in water quality surveillance, water pollution monitoring, and so on.

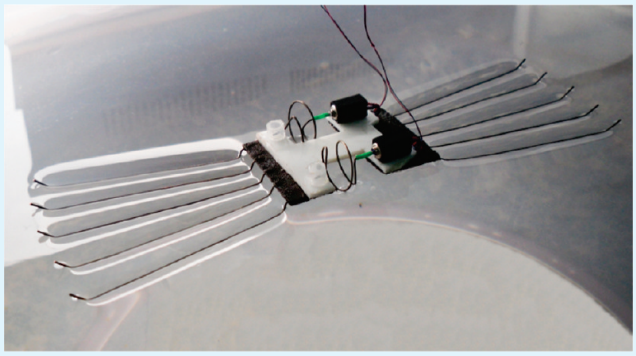

KEYWORDS: bionic aquatic microrobot, water strider-like, walking on water surface, supporting force, numerical model, mechanism

INTRODUCTION

Walking on the water surface is a great dream of humans from ancient to modern times. Although this dream is still far beyond reach of humans, walking on the water is exactly the lifestyle for some aquatic insects such as the water strider, mosquito, and water spider, etc. In nature, water striders walk and even jump on the water surfaces of ponds, slow streams, and marshes without drowning, which offer a new strategy to fabricate smart and advanced microrobotic systems that can maneuver on the water surface.[1] Therefore, trying to understand and mimic the agile behavior of water striders on the water surface is becoming an interesting topic of multidisciplinary research areas.[2]

Recently, Hu et al[3,4] demonstrated that the hydrodynamics of water striders locomotion mainly arises from the curvature force of water because the buoyancy force associated with their slim legs is too small to be taken into account. In fact, the legs of water striders form swirling vortices on the water surface, which enables them to gain momentums like the oars of a rowing boat. More recently, Jiang et al[5] reported that the origin for the curvature force associates with the superhydrophobicity of the water strider's legs. By using scanning electron microscopy, they observed a large number of ordered hierarchical hairs with fine nanogrooves covered on the surfaces of their legs. These hierarchical micrometer and nanometer structures, combined with low surface energy waxy coatings, trap a small cushion of air (known as a *plastron*) and exhibit extremely high water repellence. The plastron effect not only greatly increases the water displacement but also significantly reduces the fluid drag of the water strider's legs. Consequently, the nonwetting air cushion formed on their legs is crucial for the water striders' ability to walk and even jump on the water surface without drowning.[6−8]

Until now, mimicking the microstructure and special wettability of the water strider's legs to fabricate bioinspired aquatic devices had attracted considerable attention from the scientific community.[9−24] Although the aquatic devices made from superhydrophobic wires (or meshes) exhibited an interesting superbuoyancy property under static conditions,[16,25−27] the motion characteristic of a water strider-like microrobot on the water surface had rarely been studied.

In this study, a bionic microrobot, which could walk freely on the water surface like a real water strider, was fabricated by using two miniature driving motors, ten superhydrophobic supporting legs, and two actuating legs. Moreover, a numerical model was established to fully understand the mechanism for the large supporting forces of the superhydrophobic legs. The finding of this study provides a kind of bioinspired microrobot that can walk on the water surface to perform various aquatic missions.

Received: April 11, 2011
Accepted: June 8, 2011
Published: June 08, 2011

Scheme 1. Structural Illustration for the Aquatic Microrobot Fabricated in This Study

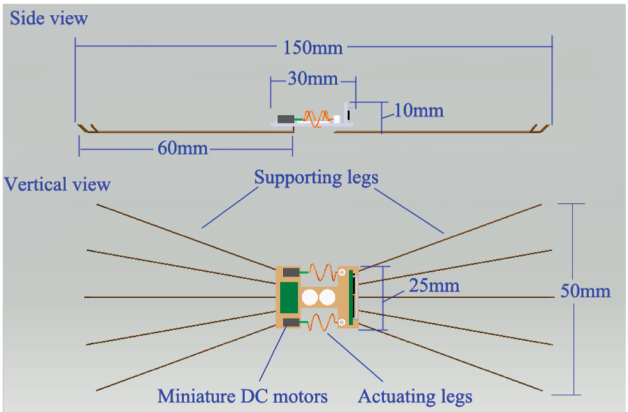

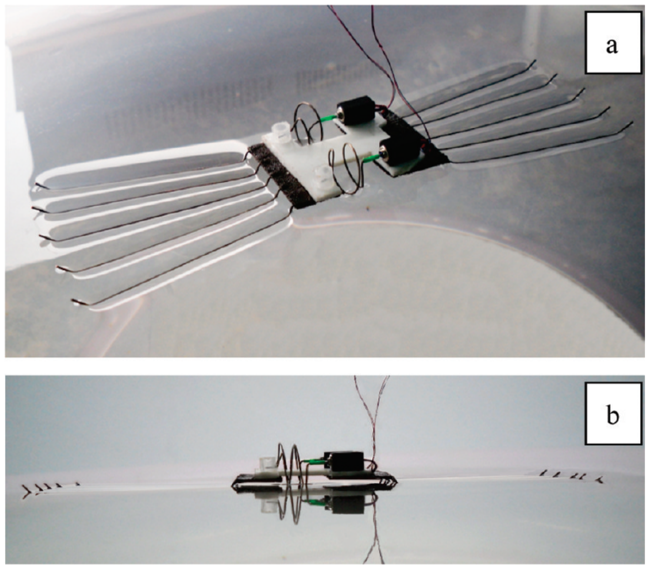

Figure 1. Top view (a) and side view (b) of the water strider-like microrobot on the surface of water.

EXPERIMENTAL SECTION

In a typical experiment, copper wires with a diameter of 500 μm were washed with a 1.0 M HCl solution and distilled water successively, then the wires were immersed into an aqueous solution containing 1.0 M NaOH and 0.05 M $K_2S_2O_8$ for 20 min.[28] After being washed with distilled water and dried, the wires were treated with an ethanol solution of 10 mM *n*-dodecanoic acid (n-$C_{11}H_{23}COOH$) for 12−72 h.[29] The obtained copper wires were subjected to further characterizations and applications. The chemical reactions involved in the above processes are described as follows:

$$Cu + K_2S_2O_8 + 2NaOH \rightarrow Cu(OH)_2 + Na_2SO_4 + K_2SO_4 \quad (1)$$

$$Cu(OH)_2 + 2n\text{-}C_{11}H_{23}COOH \rightarrow Cu(COOC_{11}H_{23})_2 + 2H_2O \quad (2)$$

To evaluate the wettability of the resulting copper wires, water contact angle (CA) measurements were conducted on a flat copper plate fabricated through the same procedures as the copper wires by using a commercial instrument (OCA 20, DataPhysics Instruments GmbH, Filderstadt). A distilled water droplet of 4 μL was used as the indicator. Scanning electron microscopy (SEM) images were obtained with an H-7650 microscope. X-ray diffraction (XRD) analysis was carried out by using a Shimadzu XRD-6000. X-ray photoelectron spectroscopy (XPS) was recorded on a PHI-5700ESCA instrument.

Then a water strider-like microrobot was fabricated according to the illustration in Scheme 1. The microrobot consists of two miniature driving motors, ten artificial supporting legs, and two actuating legs. The robot is about 15 cm long and weighs 3.88 g, which is much larger and heavier than a real water strider (about 10 mg). The length of the rowing segment of an artificial leg is about 6 cm. The weight and power output of a dc motor are 0.25 W and 0.36 g, respectively. The power and control orders are sent via the external wires that are connected to the control circuit. The actuating legs are connected to the motors, which propel the robot forward or backward when the miniature dc motors operate. The robot will turn left or right on the water surface if only one of the two motors works.

RESULTS AND DISCUSSION

First, we investigate the floating behavior of the microrobot on the water surface. Because the weight of the microrobot is equal to those of about 390 water striders, one may expect that it will sink quickly when placed on the water surface. However, it is interesting to observe that the robot stands effortlessly on the water surface with its slim supporting legs (Figure 1). The maximal supporting ability of the legs of the robot reaches 9.73 g, which dramatically exceeds the maximum buoyancy forces produced by the legs themselves. More importantly, the surface coatings on the ten legs are calculated to be only 10 mg in mass, while they can maximally support 9.73 g of weight on the water surface. The above results indicate that other forces instead of the buoyancy force support the robot.

In early studies, Hu et al[3,4] reported that vortical structures were found in the wake of water striders' legs. By forming swirling vortices on the water surface, the legs of water striders gain the momentum that propels the insect to walk on the water surface. Indeed, optical images taken from the side of the robot clearly illustrate dimples around the legs, as shown in panel (a) of Figure 2. More interestingly, the legs keep floating on the water even if they are below the water surface to some extent. Contrary to the slim supporting legs, the characteristic diameter and vertical depth of the dimples reach approximately 6.5 ± 0.2 mm and 3.2 ± 0.2 mm (Figure 2b), respectively, indicating the striking water repellency of the legs' surfaces on the water surface (i.e., plastron effect). The maximal vertical depth for a supporting leg to penetrate the water surface is estimated to be 3.6 ± 0.2 mm, consistent with the previous results.[10,25,27] The volume of a water dimple is calculated to be at least 0.97 cm^3, which is more than 70 times that of a single supporting leg. In this point, we reasonably conclude that the large supporting force for the microrobot arises from the plastron effect of the legs.

Interestingly, the robot cannot only stand effortlessly but also walk freely on the water surface. With the driving force produced by the miniature motors, the robot walks here and there on the water surface freely using the actuating legs like a real water strider, with a speed of 15 cm s^{-1} (see the movie in the Supporting Information). The robot even turns right or left on the water surface in a few seconds if only one of the motors works (see the movie in the Supporting Information). Although the speed and agility of the robot are not comparable to a real water strider, the present results still offer a possibility to fabricate microrobots capable of walking on water

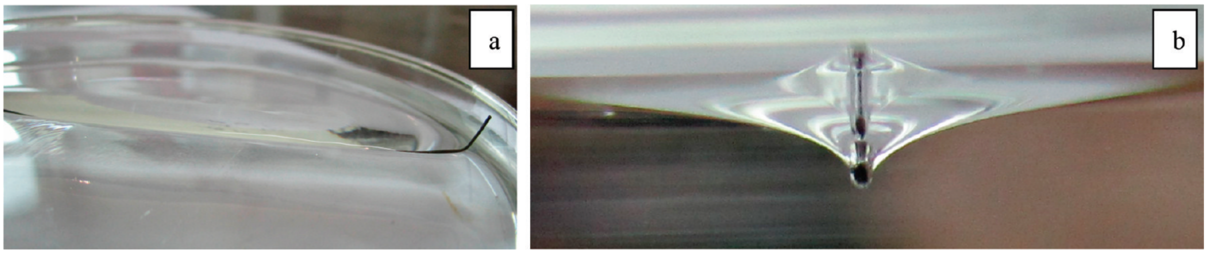

Figure 2. Optical images of top view (a) and cross section view (b) of an artificial leg on the water surface.

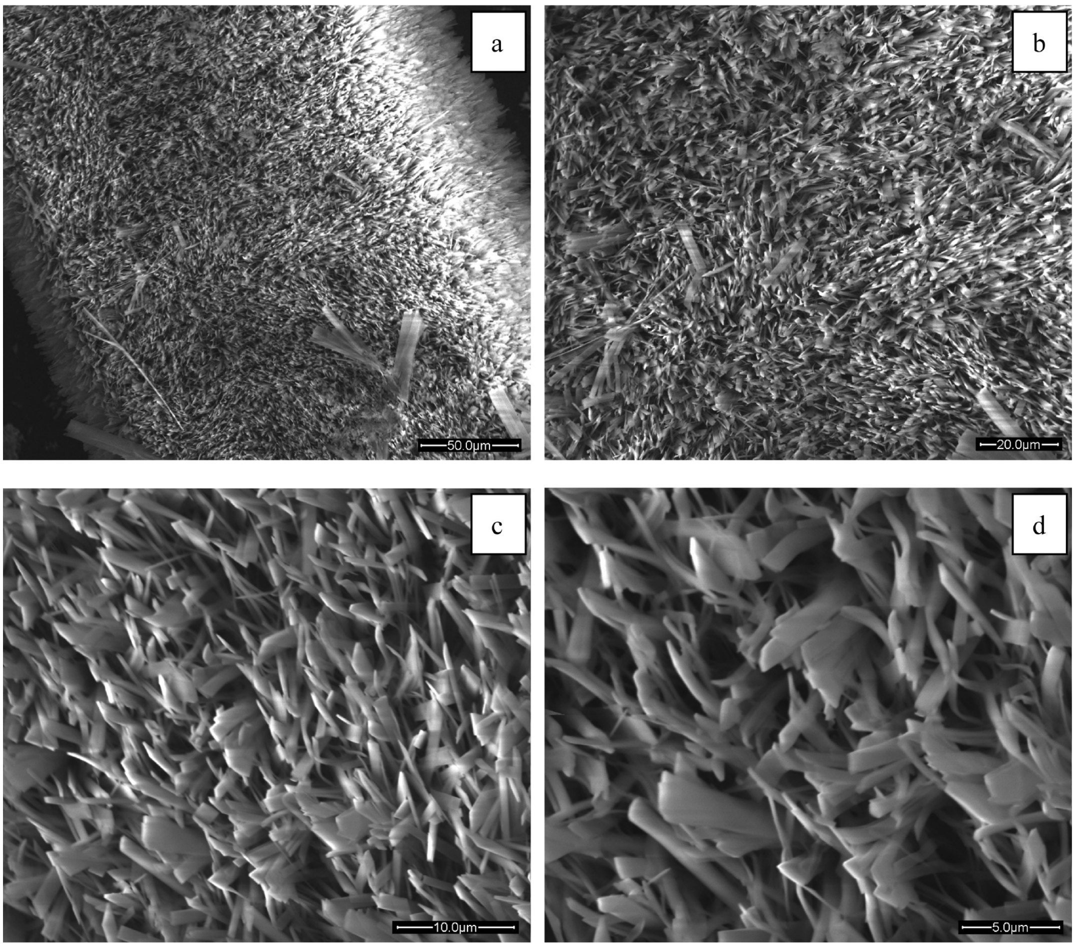

Figure 3. SEM images of nanoribbon formed on the surfaces of artificial legs: (a) × 500, (b) × 1 000, (c) × 3 000, (d) × 5 000.

by utilizing superhydrophobic wires as supporting legs and miniature motors as driving systems. Because of its low cost, desirable speed, and agility, when equipped with a miniature camera, this aquatic microrobot might have a great potential application in water pollution monitoring and military surveillance, etc.

The plastron effect of the supporting legs is believed to mainly originate from the nanoribbons formed on copper wires, as shown in Figure 3. The whole surfaces of the copper wires are covered with semioriented nanoribbons, with a length of 5−7 μm, around 2.0 μm in width, and a few hundreds nanometers in thickness. The chemical composition of the nanoribbons was identified to be $Cu(OH)_2$ by X-ray diffraction (Figure 4a).

After modification with *n*-dodecanoic acid, the surfaces of $Cu(OH)_2$ nanoribbons changed to $Cu(OOCC_{11}H_{23})_2$, as demonstrated by X-ray photoelectron spectroscopy. In Cu 3d spectrum (Figure 4b), a feature peak assigned to Cu(II) is located at 932.5 eV. In C 1s spectra, signals ascribed to the carbon atoms of C−C, $-COO^-$ and $C-COO^-$ are observed at 284.6, 288.4, and 285.3 eV (Figure 4c), respectively, indicating the existence of carbonate moiety. In addition, a characteristic peak for the oxygen atom of carbonate is observed at 532.9 eV in the O 1s spectrum (Figure 4d). The above results confirm the formation of cupric carbonate after modification with *n*-dodecanoic acid. It should be noted that the O 1s peaks at 530.6 and 531.6 eV can be attributed to the oxygen atoms of O_2 and CuO, respectively. It is believed that

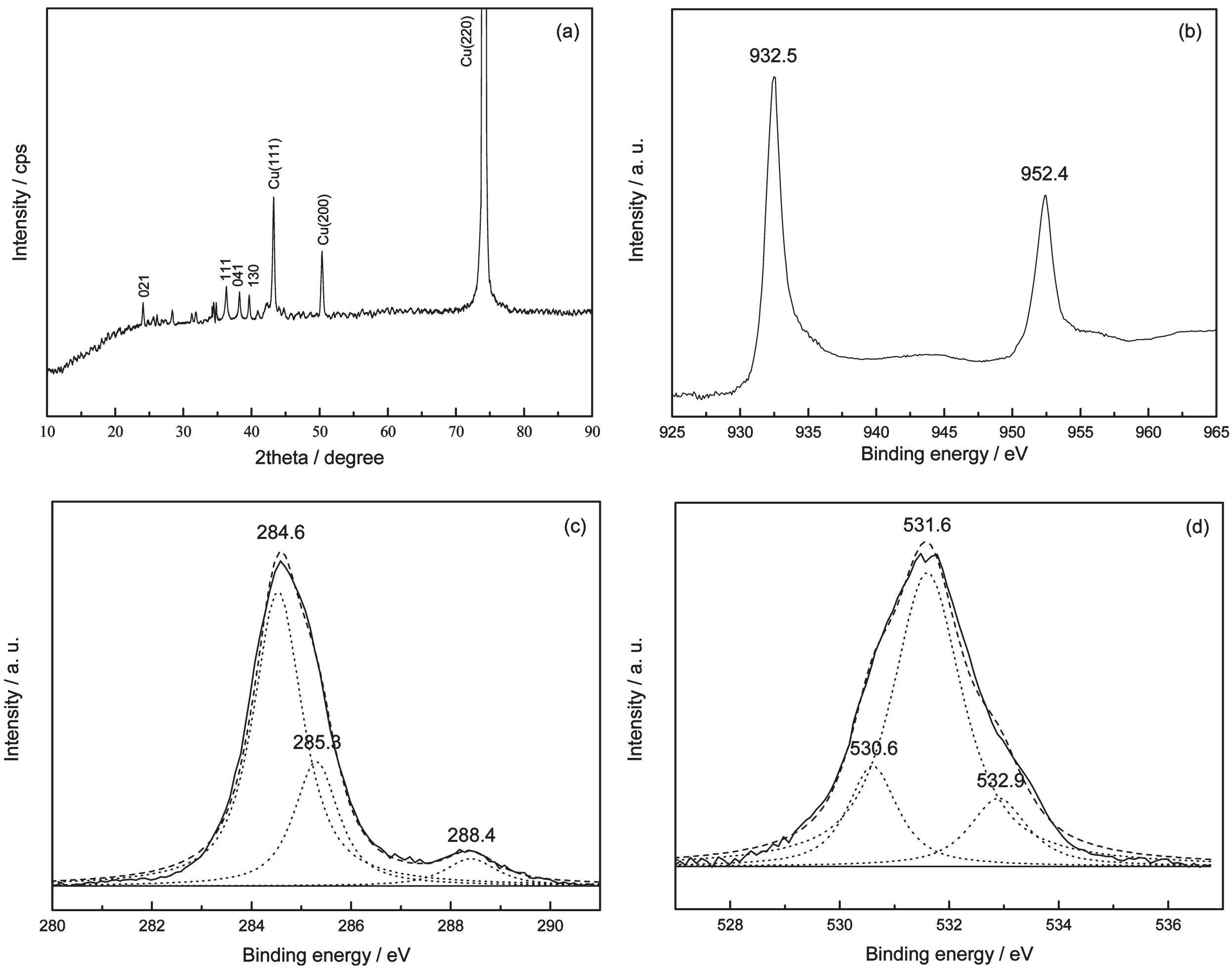

Figure 4. XRD pattern (a) of the copper wires after immersion in NaOH/$K_2S_2O_8$ solution. XPS spectra of the superhydrophobic copper wires: (b) Cu 3d, (c) C 1s, (d) O 1s.

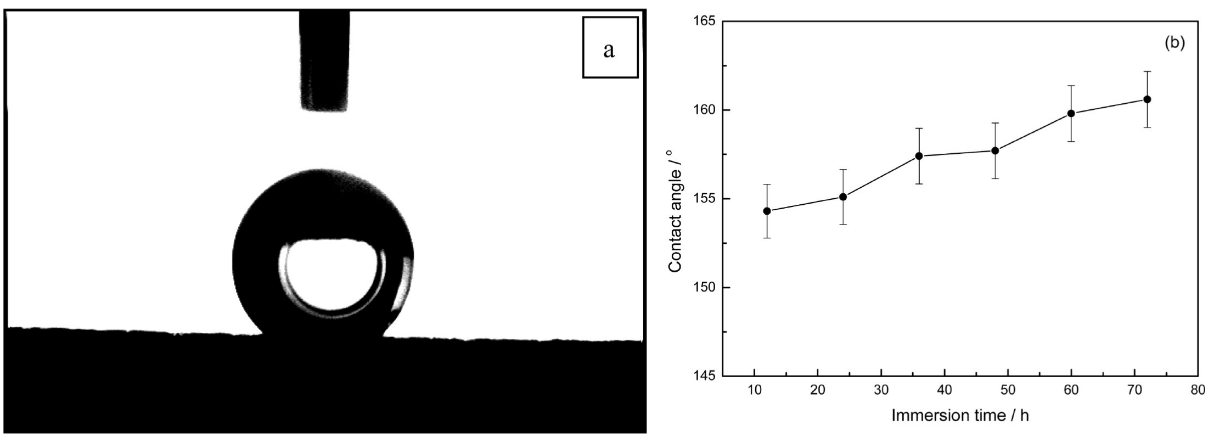

Figure 5. Typical optical image of a water droplet on the surface of a superhydrophobic copper plate prepared under the same conditions as the copper wires (a). Panel (b) is the effect of immersion time in *n*-dodecanoic acid on the water contact angles of the superhydrophobic copper plates.

the ordered nanoribbons together with low surface energy alkyl groups of $Cu(OOCC_{11}H_{23})_2$ trap a cushion of air, resulting in the plastron effect of the legs on a water surface. Although it is difficult to directly measure the water contact angle of the copper wires, a similar measurement was conducted on a flat copper plate prepared under the same conditions as the copper wires. Contact angles greater that 150° and sliding angles lower than 5° can be obtained under these conditions, confirming the superhydrophobicity of the copper plate (Figure 5a). Meanwhile, the immersion time in *n*-dodecanoic acid/ethanol solution also plays a role in the water contact angles of the copper plate. Prolonged immersion time in the ethanol solution leads to higher superhydrophobicity for the copper plate. Despite the fact that the fabrication of superhydrophobic copper wires had been reported previously,[30] the present process still has the advantages of easy fabrication, without the use of special equipments and toxic chemicals.

As discussed above, the supporting force for the microrobot mainly arises from the plastron effect of the supporting legs. To full understand the origin for the supporting force, we established a numerical model describing the interface between a partially submerged leg and the air−water surface, as shown in Scheme 2.[31] The definitions for the symbols in Scheme 2 are listed in Table 1.

By solving Young−Laplace equation,[31] we obtain a mathematical model describing the air−water interface shown in Scheme 2:

$$\begin{cases} h = 0 & (\beta = 180° - \theta_c) \\ x = \sqrt{4k - h_0^2} - \sqrt{4k - h^2} + \sqrt{k}\,lg\dfrac{\left|h_0\right|\left(2\sqrt{k} + \sqrt{4k - h^2}\right)}{\left|h\right|\left(2\sqrt{k} + \sqrt{4k - h_0^2}\right)} & (0° \le \beta \le 270° - \theta_c, \beta \ne 180° - \theta_c) \\ x = \sqrt{2k} - \sqrt{4k - h^2} + \sqrt{k}\,lg\dfrac{2\sqrt{k} + \sqrt{4k - h^2}}{\left(1 + \sqrt{2}\right)\left|h\right|} & (\beta > 270° - \theta_c) \end{cases} \quad (1)$$

where

$$h_0 = -2\sqrt{k}sin\frac{\theta_c + \beta - 180°}{2}$$

and h is the height from the original water surface, h_0 is the height between the 3-phase contact line (P_c) and the original water surface, $k = \gamma/\rho g$, $\rho = \rho_1 - \rho_2$, and γ, g is the surface tension coefficient and gravitational constant, respectively. The shapes of the air−water interfaces with different h_0 can be well estimated from eq 1. Panel (a) of Figure 6 shows the shape variation of the air−water interfaces in the process of a leg immersing into water surface. The radius (r) and contact angle (θ_c) of the legs are 250 μm and 155.8°, respectively. The results clearly display that the shape of the air−water interface is strongly dependent on the height (h_0) between the leg and the original water surface.

On the basis of the numerical model in Scheme 2, the total supporting force (F) relates to the weight of the water dimple that can be compartmentalized into the vertical component of the surface tension (F_σ) and buoyancy force (F_b),[32−34] which can be described as

$$F = 2F_\sigma sin(\theta_c + \beta - 180°) + F_b \quad (2)$$

where

$$\begin{cases} F_\sigma = \gamma l \\ F_b = \rho gl(-2h_0 rsin\,\beta + \beta r^2 - r^2 cos\,\beta sin\,\beta) \end{cases}$$

and l is the length of the rowing segment of the leg. Equation 1 implies that the total supporting force (F) will be determined by eq 2 for a given submerge angle (β). Panel (b) of Figure 6 plots the dependence of the supporting force (F) and submerge angle (β) on the height (h_0). It is shown that a maximum supporting force (F_{max}) of 1.59 mN cm^{-1} is obtained when h_0 is equal to −3.8 mm and the corresponding β is about 115°. Consequently, the maximum supporting force (F_{max}) provided by the ten legs (l = 60 mm) is numerically estimated to be 95.4 mN (i.e., 9.73 g), which sufficiently supports this aquatic microrobot on the water surface.

Equation 2 also indicates that the radius (r) and contact angle (θ_c) of the legs have an impact on the supporting force (F). Panel

Scheme 2. Cross Section Model of the Air−Water Interface of a Partially Submerged Leg

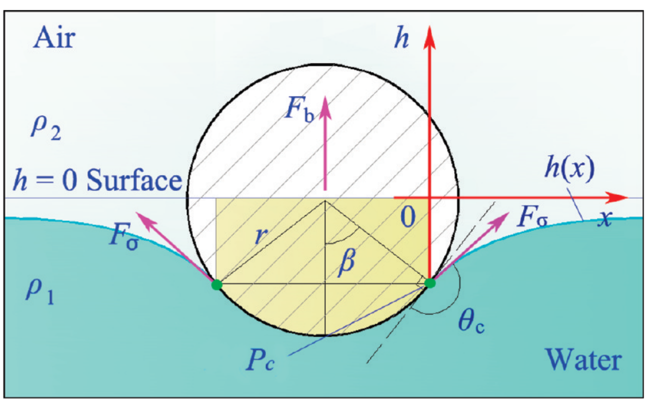

Table 1. Definitions for the Symbols in Scheme 2

symbols	notation
θ_c	contact angle
ρ_1	density of water
ρ_2	density of air
r	radius of leg
β	submerge angle
F_b	buoyancy force
F_σ	surface tension force
P_c	3-phase contact line

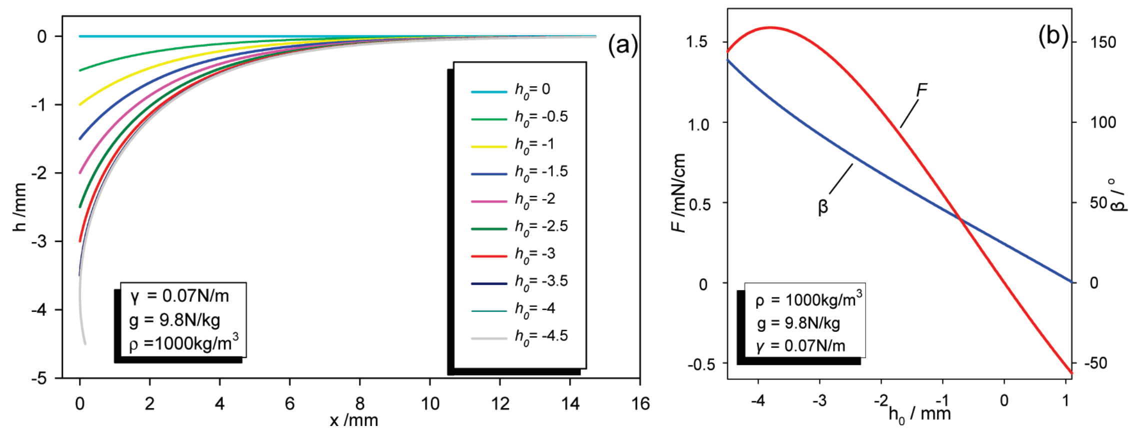

Figure 6. (a) Illustrations for the shapes of the air−water interface in the process of a leg immersing into water surface, and (b) dependence of the supporting force (F) and submerge angle (β) on the height (h_0).

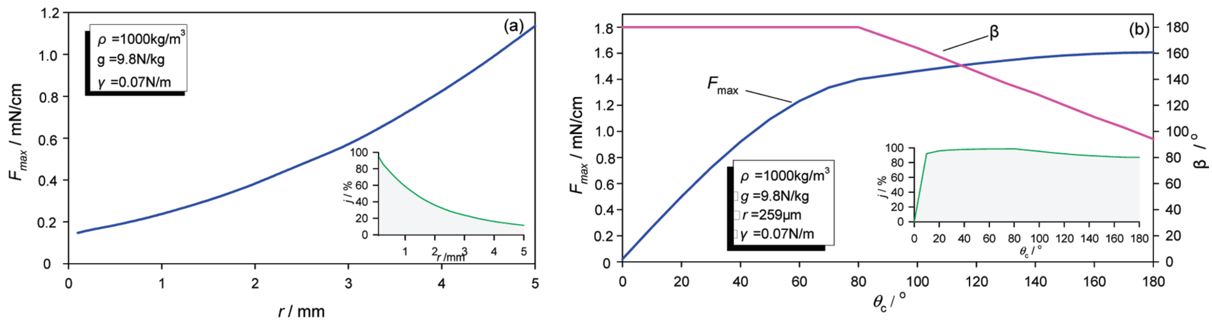

Figure 7. (a) Influence of the radius (r) of legs on the maximum supporting force (F_{max}). (b) Effect of contact angle (θ_c) on the maximum supporting force (F_{max}) and submerge angle (β). Insets are the proportions (j) of surface tension (F_σ) in the maximum supporting force (F_{max}).

(a) Figure 7 shows the relationship between the maximum supporting force (F_{max}) and r, as well as the proportion (j) of surface tension (F_σ) in F_{max}. It is revealed that an increase in the radius (r) results in a larger F_{max}, while the contribution of surface tension (F_σ) to F_{max} decreases as the radius increases from 0.1 to 5 mm. The proportion (j) of surface tension (F_σ) exceeds that of buoyancy force (F_b) when the radius is below 1.0 mm. Panel (b) of Figure 7 illustrates the effect of the water contact angle (θ_c) on F_{max}. Generally, F_{max} grows continuously with increasing θ_c, confirming the significance of superhydrophobicity on the supporting force of the legs. The above results explain the reasons that account for the large supporting force of the microrobot's legs.

■ CONCLUSIONS

In summary, this study reported a new kind of aquatic microrobot that could walk freely on the water surface like a real water strider. The microrobot was supported by ten superhydrophobic artificial legs and driven by two actuating legs that connected to two miniature dc motors. The mechanism for the large supporting force of the artificial legs was theoretically explained by a numerical model. It was revealed that the radius and contact angle of the legs mainly accounted for the large supporting force, ensuring that the robotic water strider not only stood but also walked on the water surface. Our investigation offers a facile process to assemble novel microrobots that can walk on the water surface by using superhydrophobic wires and miniature motors. We anticipate that this bioinspired aquatic microrobot might find its potential application in aquatic missions, including water pollution monitoring and water quality surveillance, etc.

■ ASSOCIATED CONTENT

S Supporting Information. Video showing the movement of the microrobot on water surface. This information is available free of charge via the Internet at http://pubs.acs.org.

■ AUTHOR INFORMATION

Corresponding Author
*E-mail: panqm@hit.edu.cn.

■ ACKNOWLEDGMENT

This work was financially supported by a self-planned task of The State Key Laboratory of Robotics and System of Harbin Institute of Technology (SKLRS200901C) and Natural Science Foundation of China (NSFC, Grant 50803013). The authors express their gratitude to Professor Yang Gan for the measurement of water contact angles.

■ REFERENCES

(1) Wilcox, R. S. *Science* **1979**, *206*, 1325–1327.
(2) Sun, T.; Feng, L.; Gao, X.; Jiang, L. *Acc. Chem. Res.* **2005**, *38*, 644–652.
(3) Hu, D. L.; Chan, B.; Bush, J. W. M. *Nature* **2003**, *424*, 663–666.

(4) Hu, D. L.; Bush, J. W. M. *Nature* **2005**, *437*, 733–736.
(5) Gao, X. F.; Jiang, L. *Nature* **2004**, *432*, 36–36.
(6) Wu, C. W.; Kong, X. Q.; Wu, D. *Phys. Rev. E* **2007**, *76*, 017301.
(7) Feng, X. Q.; Gao, X. F.; Wu, Z. N.; Jiang, L.; Zheng, Q. S. *Langmuir* **2007**, *23*, 4892–4896.
(8) Goodwyn, P. P.; De Souza, E.; Fujisaki, K.; Gorb, S. *Acta Biomater.* **2008**, *4*, 766–770.
(9) Pan, Q. M.; Wang, M. *ACS Appl. Mater. Interfaces* **2009**, *1*, 420–424.
(10) Pan, Q. M.; Liu, J.; Zhu, Q. *ACS Appl. Mater. Interfaces* **2010**, *2*, 2026–2030.
(11) Miwa, M.; Nakajima, A.; Fujishima, A.; Hashimoto, K.; Watanabe, T. *Langmuir* **2000**, *16*, 5754–5760.
(12) Wang, R.; Hashimoto, K.; Fujishima, A.; Chikuni, M.; Kojima, E.; Kitamura, A.; Shimohigoshi, M.; Watanabe, T. *Nature* **1997**, *388*, 431–432.
(13) Zhang, X.; Kono, H.; Liu, Z.; Nishimoto, S.; Tryk, D. A.; Murakami, T.; Sakai, H.; Abe, M.; Fujishima, A. *Chem. Commun.* **2007**, 4949–4951.
(14) Wang, R.; Hashimoto, K.; Fujishima, A.; Chikuni, M.; Kojima, E.; Kitamura, A.; Shimohigoshi, M.; Watanabe, T. *Adv. Mater.* **1998**, *10*, 135–138.
(15) Yu, S. H; Colfen, H; Antonietti, M. *Adv. Mater.* **2003**, *15*, 133–136.
(16) Larmour, I. A.; Saunders, G. C.; Bell, S. E. J. *Angew. Chem., Int. Ed.* **2008**, *47*, 5043–5045.
(17) Yu, S. H.; Colfen, H.; Tauer, K.; Antonietti, M. *Nat. Mater.* **2005**, *5*, 51–55.
(18) Larmour, I. A.; Bell, S. E. J.; Saunders, G. C. *Angew. Chem., Int. Ed.* **2007**, *46*, 1710–1712.
(19) Yang, J.; Xue, C.; Yu, S. H.; Zeng, J. H.; Qian, Y. T. *Angew. Chem. Ed. Int.* **2002**, *41*, 4697–4700.
(20) Yu, S. H.; Antonietti, M.; Colfen, H.; Hartmann, J. *Nano Lett.* **2003**, *3*, 379–382.
(21) Hu, D. L.; Chan, B.; John, W. M. *Elsevier Science* **2005**, *6*, 256–263.
(22) Gao, T. H; Zhu, D. Y; Cao, J. Y.; Qin, Y. X. *IEEE Int. Conf. Rob. Biomimetics* **2007**, *1*−*5*, 775–780.
(23) Gao, T. H; Cao, J. Y; Zhu, D. Y.; Zhi, J. Z. *Proceedings IEEE Int. Conf. Integr. Technol.* **2007**, 685–690.
(24) Solovev, A. A.; Mei, Y. F.; Schmidt, O. G. *Adv. Mater.* **2010**, *22*, 4340.
(25) Shi, F.; Niu, J.; Liu, J.; Liu, F.; Wang, Z.; Feng, X.; Zhang, X. *Adv. Mater.* **2007**, *19*, 2257–2261.
(26) Shi, F.; Wang, Z. Q.; Zhang, X. *Adv. Mater.* **2005**, *17*, 1005–1009.
(27) Jiang, L.; Yao, X.; Li, H.; Fu, Y.; Chen, L.; Meng, Q.; Hu, W.; Jiang, L. *Adv. Mater.* **2010**, *22*, 376–379.
(28) Pan, Q. M.; Wang, M.; Wang, H. B. *Appl. Surf. Sci.* **2008**, *254*, 6002–6006.
(29) Pan, Q. M.; Jin, H. Z.; Wang, H. B. *Nanotechnology* **2007**, *18*, 355605.
(30) Wu, X. F.; Shi, G. Q. *J. Phys. Chem. B* **2006**, *110*, 11247–11252.
(31) Song, Y. S.; Suhr, S. H.; Sitti, M. *Robotics and Automation* **2006**, *5*, 2303–2310.
(32) Finn, R. *Equilibrium Capillary Surfaces*; Springer: Berlin, 1986.
(33) Keller, J. B. *Phys. Fluids* **1998**, *10*, 3009–3010.
(34) Suzuki, K.; Takanobu, H.; Noya, K.; Koike, H.; Miura, H. Proceedings of the IEEE/RSJ International Conference on Intelligent Robots and Systems (IROS07), San Diego, CA, 2007, pp 590−595.